ICARUS **132,** 205–220 (1998)
ARTICLE NO. IS985898

Interpretation of Galileo Probe Data and Implications for Jupiter's Dry Downdrafts

Adam P. Showman and Andrew P. Ingersoll

Division of Geological and Planetary Sciences 150-21, California Institute of Technology, Pasadena, California 91125
E-mail: showman@earth1.gps.caltech.edu

Received July 29, 1997; revised December 4, 1997

The Galileo probe found the jovian abundance of H_2S to be 30% solar at the 8 bar level, while the abundance of water was less than 3% solar at 12 bars. From 8 to 20 bars, H_2S increased to three times solar, and water apparently increased as well. Since H_2S and water condense at 2 and 5 bars, respectively, the probe probably entered a dry downdraft, wherein dry air above 2 bars is advected to 12 bars or deeper (Owen *et al.* 1996, *Eos* (Spring Suppl.) 77, S171). This is consistent with the fact that the probe entered the south edge of a 5-μm hot spot, a local region of Jupiter's atmosphere known from spectral modeling to be unusually low in cloud abundance (Orton *et al.* 1996, *Science* 272, 839).

We use basic physical constraints to address three problems raised by Galileo probe data. First, it is unclear how the hypothesized downdraft remains dry, since simple models of convection preclude dessication below the 2- and 5-bar condensation levels. We suggest that to suppress moist plumes from below, the downdraft must be of low density below 5 bars and hence thermally indirect, requiring mechanical forcing from other parts of the atmosphere. Second, if geostrophic balance holds, the Galileo probe winds imply that the hot spot (north of the probe site) contains a stable layer from 1 to 5 bars; this is inconsistent with a downwelling, since downwellings should be adiabatic below 2 bars due to the low radiative flux divergence. We show that when the centripetal acceleration of curving parcel trajectories is included in the force balance, however, a variety of density profiles is possible within the hot spot (depending on the radius of curvature of the winds). The most plausible profile implies that the hot spot is nearly dry adiabatic and that the equatorial zone south of the probe site is stable from 2 to 6 bars, suggesting moist adiabatic upwellings with a water abundance of 1–2 times solar. This is consistent with Galileo and Voyager images suggesting upwelling at the equator. The profile further implies that from 1 to 5 bars the hot spot is denser than the equatorial zone south of the probe site. Third, probe data indicate that NH_3 increased with depth below 1 bar and became constant by 8 bars, H_2S began increasing below 8 bars and leveled off by 16 bars, while water only began increasing below 12 bars and was still increasing with depth at 20 bars. We propose that lateral mixing along isopycnals (surfaces of constant potential density) could produce the observed pattern; alternatively, the downwelling might consist of column stretching, so that the NH_3, NH_4SH, and water lifting condensation levels were pushed to 8, 16, and >20 bars, respectively. In either case, the simplest form of this model requires the downdraft to be less dense than the surroundings from 0.5 to 20 bars. In its simplest form, this model is therefore incompatible with our favored interpretation of the winds; more detailed studies will be necessary to resolve the problem. © 1998 Academic Press

Key Words: **Jupiter (atmosphere); atmospheres (dynamics); atmospheres (structure); spacecraft.**

1. INTRODUCTION

The Galileo probe took *in situ* measurements of Jupiter's atmosphere from the 0.4-bar level, near the visible cloud tops, to the 20-bar level, 150 km deeper. Among the measurements came the surprising result that the H_2S mole fraction at the 8-bar level was 1×10^{-5}, while the water vapor mole fraction at 12 bars was 6×10^{-5} or less (Niemann *et al.* 1996, 1997, Atreya 1996). These values are roughly 30% and <3% of "solar" abundance, defined as solar S/H and O/H mixtures with the sulfur and oxygen speciated into H_2S and H_2O, as expected for Jupiter's atmosphere. These results are puzzling because Jupiter probably formed from a reservoir with solar or greater S/H and O/H (Gautier and Owen 1989); further, between 8 and 16 bars, H_2S surged from 0.3 to 2.7 times solar, and water also apparently increased by an order of magnitude between 12 and 20 bars (although the absolute water abundance is still uncertain at depth; Niemann *et al.* 1997, Mahaffy 1996). Global depletion of these volatile species is therefore ruled out. Condensation cannot explain the low abundances at 8 bars, because H_2S and water only condense above 2 and 5 bars, respectively, when abundances are near solar (Weidenschilling and Lewis 1973). The probe therefore apparently fell into a dry downdraft, a region where dry air from above cloud top is advected to 12 bars or deeper, producing locally dessicated conditions to those depths (Owen *et al.* 1996, Atreya 1996). Young (1997) summarizes the probe results.

0019-1035/98 $25.00

The idea of a downdraft is consistent with the fact that the probe entered the south edge of a 5-μm "hot spot," a local region in Jupiter's north equatorial belt which has unusually high 5-μm emission (Orton *et al.* 1996, 1997). The high emission emanates from deep levels, suggesting that these 10^3–10^4-km-sized spots are severely depleted in both cloud abundance (Carlson *et al.* 1994) and water and ammonia vapor (Carlson *et al.* 1996, Roos-Serote *et al.* 1997, Drossart *et al.* 1997). Further, hot spots reside within belts, where modeling of Voyager thermal data predicts downwelling (Gierasch *et al.* 1986, West *et al.* 1992). Thus, the idea that downwelling occurs within hot spots is reasonable.

However, there are problems reconciling the downdraft hypothesis with other data and basic physical constraints. In this paper, we propose solutions to three problems raised by Galileo probe data.

In Section 2, we consider the first problem: How do we keep the downdraft dry to 20 bars? Simple models of convection suggest that downdrafts are denser than updrafts. If so, moist plumes rising from Jupiter's interior should be buoyant within the downdraft and should quickly mix H_2S and water vapor up to the condensation levels at 2 and 5 bars. In order for the downdraft to remain dry, upward transport of moist plumes must be suppressed. The subsiding air must therefore be underlain by a stable layer, and must be *less dense* than the surroundings. This implies that the circulation is thermally indirect (updrafts denser than downdrafts). Such circulations increase the atmosphere's potential energy; we show that this increase can be driven either by loss of kinetic energy or by a flux of geopotential energy from another part of the atmosphere. We describe several mechanisms for creating the low density air. Indirect circulations have already been proposed to exist above the ammonia cloud tops on Jupiter (Gierasch *et al.* 1986), and are important on Earth.

The second problem, considered in Section 3, is explaining the probe winds. The probe measured eastward winds of 90 m s^{-1} at cloud top, increasing to 180 m s^{-1} at 5 bars, then decreasing slightly to 170 m s^{-1} at 20 bars (Atkinson *et al.* 1996, 1997). Because of Jupiter's high rotation rate and large size, atmospheric features are normally thought to be in geostrophic balance, a balance between pressure-gradient and Coriolis forces. When combined with hydrostatic balance, the well-known "thermal wind" relation results (Holton 1992, p. 73). This equation relates the vertical wind profile to the latitudinal gradient of density with depth at the probe site. The fact that $\partial u/\partial p > 0$ from 1 to 5 bars implies that over this pressure range the hot spot (north of the probe site) is less dense than the equatorial zone (south of the probe site); further, the slightly decreasing winds from 5 to 20 bars suggest that the hot spot is marginally denser than the equatorial zone in that layer. The hot spot is therefore statically stable from 1 to 5 bars. This is difficult to reconcile with downwelling in the hot spot, because subsiding regions should be dry adiabatic below 2 bars, where the net radiative flux divergence is low (Sromovsky *et al.* 1996, 1997, Hunten *et al.* 1980).

To resolve this problem, we show that geostrophic balance may not hold. At the probe site's equatorial latitude of 6.5°N, the Coriolis force is relatively weak and the centripetal force due to curving wind trajectories becomes important. This invalidates the thermal wind equation. Using a generalization of the equation valid for gradient wind balance (a balance between pressure-gradient, Coriolis, and centripetal forces), we calculate possible vertical profiles of the latitudinal density gradient. The profiles depend on the local radius of curvature of the winds, which is poorly known. For certain values of the radius of curvature, the hot spot is denser than the equatorial zone in the 1–5 bar layer, but is less dense than the equatorial zone in the 5–12 bar layer. These gradients therefore predict a stable layer from 1 to 5 bars *south* of the probe site, where modeling of Voyager data suggests upwelling (Gierasch *et al.* 1986), and allow the hot spot to be dry adiabatic below 2 bars, consistent with a downwelling. This resolves the problem.

In Section 4 we attack another vexing observation, shown in Fig. 1—that NH_3 increased rapidly below 1 bar, reaching a plateau below 8 bars (Folkner *et al.* 1998); H_2S began increasing below 8 bars and tentatively leveled off by 16 bars, while water only began increasing below 12 bars and was still increasing with depth at 20 bars (Niemann *et al.* 1997). This pattern mimics that predicted by equilibrium condensation models (Weidenschilling and Lewis 1973) but occurs at much greater pressures. Lateral mixing has been proposed by Atreya *et al.* (1997) to account for the observed pattern. However, this requires material to descend by ~50–100 km as it mixes from the surroundings into the probe site. We assume such mixing takes place on isopycnals (surfaces of constant potential density) and explore the implications. This provides a natural explanation for why horizontal mixing does not moisten the downdraft, despite the vigorous horizontal motions observed in Jupiter's atmosphere. We also offer an alternate hypothesis to explain the data in Fig. 1—that the downdraft consists simply of stretching of the air column, with no mixing.

In Section 5, we return to the question of forcing posed in Section 2. Armed with constraints on the hot spot's density versus depth developed in Sections 3 and 4, we consider the following question: Can the atmospheric heat engine supply enough energy to push dry air to 10–20 bars as observed? The data tentatively suggest that the atmospheric circulation *is* energetic enough to push dry air to 10–30 bars and possibly much deeper. This provides a consistency check that the postulated indirect circulation is energetically reasonable. However, we do not provide a detailed mechanism.

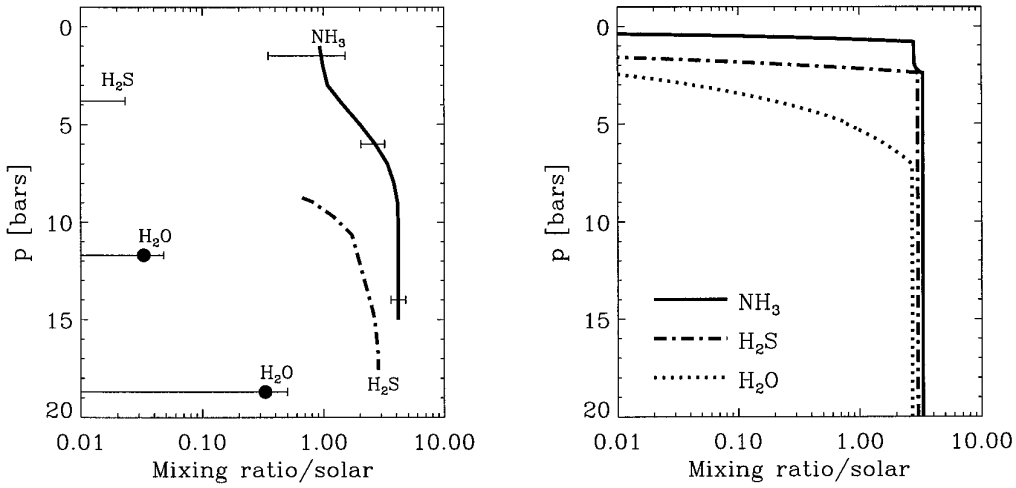

FIG. 1. (Left) Abundances of NH_3, H_2S, and H_2O vs pressure as measured by the Galileo probe. The NH_3 profile (thick solid line) is from Folkner *et al.* (1998), while the H_2S data (thick dash–dot line) and H_2O data (filled circles) are from Niemann *et al.* (1997). The filled circles represent actual detections of H_2O which are upper limits because of the possibility of outgassing from the equipment; the upper limit on H_2S at 3.8 bars is a nondetection. All data are preliminary and may be revised in the future. (Right) Profiles of NH_3 (solid line), H_2S (dash–dot line), and H_2O (dotted line) as predicted from an equilibrium condensation model, assuming deep abundances near 3 times solar. Comparison with the model shows that the observed increases with pressure cannot be caused by condensation. If they were caused by mixing from below, however, one would expect the mixing ratios of the three gases to increase together. The observed behavior is therefore puzzling.

In Section 6 we summarize our results and discuss an apparent inconsistency between our favored interpretations of the wind and mass spectrometer data.

2. PUZZLE I: KEEPING THE DOWNDRAFT DRY

For the downdraft to be dry, it must be underlain by a stable layer, so that moist plumes rising from below are suppressed. If the density is independent of horizontal position in the deep atmosphere, this implies that (just above the stable layer) the descending air is less dense than the upwellings at the same pressure.

There are two important questions we must tackle to understand this anomalous situation. First, what mechanisms exist for creating the low-density air? These mechanisms will determine how high (above the stable layer) the low-density air extends. Second, what sort of forcing is required to make such air descend? In this section, we propose possible answers. Because of the paucity of data, our aim is more to clarify the possibilities rather than espouse any particular model. We also discuss examples of indirect circulations on Earth. Finally, we compare our model to other hypotheses which have been proposed for explaining the dryness at the probe site.

2.1. Creating the Low-Density Air

Figure 2 schematically shows mechanisms for creating a low-density downdraft, by qualitatively depicting two possible thermodynamic paths followed by air which rises in the region surrounding the hot spot and descends in the hot spot. The left panel depicts the proposed circulation, while (a) and (b) show the two scenarios. In (a) and (b), the horizontal axis is virtual temperature, defined as $T_v = Tm_d/m$, where T is temperature, m_d is the mass per molecule of "dry" air (free of ammonia, H_2S, and water), and m is the mass per molecule of the mixture. Virtual temperature measures density at a given pressure: high T_v implies low density and vice versa. Both scenarios assume a homogenous deep atmosphere containing roughly solar water. The deep atmosphere extends in some regions up to the water condensation level near 5 bars, where it produces cloudiness and upwelling. Above the condensation level ($p < 5$ bars), these upwellings follow a moist adiabat; most of the condensate is assumed to rain out. The moist adiabats have smaller $|\partial T_v/\partial z|$ than a dry adiabat because of the warming and decrease of molecular mass associated with condensation and rainout; such regions are termed "statically stable." In the first scenario (a), the radiative equilibrium temperature is less than the air temperature near the ammonia cloud top. The dry downwellings therefore *cool* by radiation at $p < 2$ bar (becoming denser than the upwelling) and follow a dry adiabat below 2 bars. However, they cool insufficiently to become denser than the upwellings (and deep atmosphere) *below* the water condensation level; therefore, they are less dense than the surroundings from 5 bars to the bottom of the downdraft. If the radiative cooling is great enough, the downwelling column (averaged from 0.5 bars to the bottom of the down-

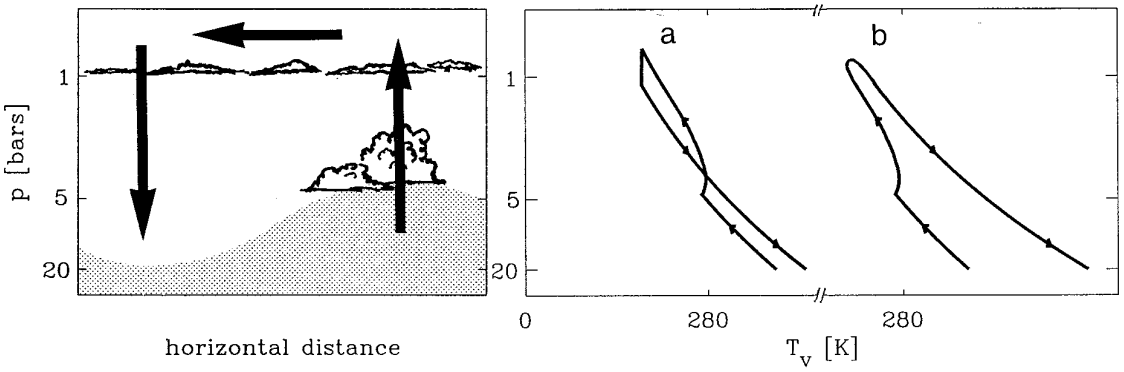

FIG. 2. A model to explain the dryness at the probe site. (Left) A schematic of our proposed circulation; arrows denote air motion and the stippled region indicates air with high water vapor content. (Right) Diagrams of two possible thermodynamic paths followed by air rising in the regions surrounding the hot spot and descending in the hot spot. The plots have the same vertical axis; the horizontal axis for the thermodynamic paths is virtual temperature. (a) Updrafts follow a moist adiabat above the 5-bar water condensation level; downdrafts *cool* by radiation above 2 bars and follow a dry adiabat below. Downdraft is less dense at $p > 5$ bars. The difference between the moist and dry adiabats has been exaggerated for clarity. (b) Updrafts follow a moist adiabat, but radiatively *warm* in upper troposphere. Downwellings follow dry adiabat. Downdrafts are less dense for $p > 0.5$ bars. Both models produce a deep stable layer which suppresses the mixing of volatiles into the downdraft.

draft) may be denser than the upwelling column. This would provide a natural mechanism for driving the downdraft; on average, the circulation would be thermally direct (downdrafts denser than updrafts).

The radiative equilibrium temperature is poorly known, however, and could be greater than the upwelling air temperature above 0.5 bars. In that case, as shown in (b), radiative *warming* occurs above 0.5 bars as the air rises. (Because net radiative cooling to space occurs at all latitudes on Jupiter, this warming must be accompanied by radiative cooling elsewhere within the column. For example, if the updrafts in Fig. 2b occur in thunderstorms, some of the downdraft air could cool radiatively while subsiding between thunderstorms. The remainder would ascend, warm radiatively [a result of having cooled adiabatically to temperatures below the radiative equilibrium temperature], and descend in the hot spot. Only the latter thermodynamic path is depicted in Fig. 2b.) When the air descends it is therefore warmer than the upwelling. In this scenario, the updrafts are denser than the dry downdrafts at all heights below ~0.5 bars. Gierasch *et al.* (1986) proposed an analogous mechanism to account for the upper tropospheric belt-zone temperature difference and cloud patterns: upwelling occurs in the (cold) zones and downwelling in the (warm) belts.

A third scenario exists. If the descent time from the tropopause to a few bars is much less than the radiative time (a few years), minimal radiative cooling or warming would occur. The downdraft and updraft would be of comparable density above a few bars, but the downdraft would be less dense at deeper levels. This scenario can be considered a special case of (b).

The two scenarios have one feature in common: the difference in virtual temperature between the downdrafts and updrafts increases with depth from ~2 to 6 bars. (For example, in (a), $T_{v,down} - T_{v,up}$ is negative at low pressures, crosses through zero near 5 bars, and becomes positive at $p > 5$ bars.) This feature will aid our interpretation of the probe winds in Section 3.

2.2. Forcing the Dry Air Downward

Atmospheric convection operates as a heat engine, converting potential energy into kinetic energy by pressure forces acting on buoyant updrafts and dense downdrafts. When high density air rises and low density air sinks, as in the present case, potential energy is increased; this increase in potential energy occurs either by destruction of kinetic energy or by work done by pressure forces created elsewhere in the atmosphere. To quantify this energetic cycle, consider the hydrostatic atmospheric kinetic energy equation from Haltiner and Williams (1980, p. 20)

$$\frac{\partial K}{\partial t} + \nabla \cdot [\mathbf{v}(K + \Phi)] + \frac{\partial}{\partial p}[\omega(K + \Phi)] = -\frac{\omega}{\rho} + \mathbf{v} \cdot \mathbf{F}, \quad (1)$$

where $K = \mathbf{v} \cdot \mathbf{v}/2$ is atmospheric kinetic energy per mass, $\mathbf{v}$ is the horizontal wind vector, $\omega = dp/dt$ is the vertical velocity in pressure coordinates, Φ is geopotential, ρ is density, p is pressure, $\mathbf{F}$ is the frictional drag force, and $\nabla = (\partial/\partial x, \partial/\partial y)$. The term $-\omega/\rho$ represents conversion of potential energy into kinetic energy by pressure forces. (This conversion can be seen by considering the hydrostatic enthalpy equation from Haltiner and Williams

$$\frac{\partial H}{\partial t} + \nabla \cdot (\mathbf{v}H) + \frac{\partial(\omega H)}{\partial p} = \frac{\omega}{\rho} + Q, \tag{2}$$

where H is enthalpy per mass and Q is heating by radiation, conduction, and viscous dissipation of kinetic energy.) Returning to the kinetic energy equation, we average in the horizontal over a local area around the indirect circulation and integrate over mass from a lower pressure p_{bot} (below the bottom of the dry downdraft) to an upper pressure p_{top} of 270 mbar near the tropopause. Rearranging, the equation becomes

$$\int \frac{1}{\rho}\frac{dp}{dt}\,dm = -\int \dot{K}\,dm - \int \left(\frac{1}{A}\int_{\text{sides}} (K+\Phi)\,\mathbf{v}\cdot\mathbf{n}\,dl\right) dm - \frac{1}{g}[\omega(K+\Phi)]_{\text{top}} + \frac{1}{g}[\omega(K+\Phi)]_{\text{bottom}} - D, \tag{3}$$

where D is the dissipated power per area in the volume, $\mathbf{n}$ is the outward normal vector, and A is the horizontal area of the domain. The integration element dm is mass per area and dl is distance (along an isobar) around the sides of the volume. The left side of the equation is a measure of the change in gravitational (and internal) energy brought about by atmospheric motion. It is the difference between the power stored in the thermally indirect parts of the circulation and that released in the thermally direct parts (it is positive if thermally indirect circulations dominate and negative if direct ones dominate).

The equation states that creation of column integrated enthalpy by atmospheric motion (as would occur in an indirect circulation) is balanced by importation of kinetic and geopotential energy into the volume minus the power per area lost to dissipation or stored as kinetic energy. In steady state, therefore, the indirect circulation can be forced by importation of either kinetic or geopotential energy through the boundaries. In the former case, the imported kinetic energy is created by pressure forces elsewhere in the fluid; in the latter case, these pressure forces do work directly on the indirect circulation without any intermediate generation of kinetic energy. If the downwelling column is denser than the upwelling column (as could be the case in Fig. 2a), the net circulation is thermally direct, doing work on the environment. In this case, the thermally indirect motion below 5 bars is driven by geopotential energy flux (through the 5 bar surface) from the overlying direct motion.

The best example of an indirect circulation powered by importation of geopotential energy is the lower stratospheric circulation on Earth. The upwelling air at the equator cools so much by adiabatic expansion that it becomes colder than the subsiding air at higher latitudes; this atmospheric motion creates enthalpy, which is destroyed by radiation (Tomatsu 1979). Near the tropopause, the isobars bow upward, where upwelling occurs and downward where downwelling occurs. This leads to importation of geopotential energy across the 150 mbar surface at a rate of 0.3 W m^{-2} (Tomatsu 1979). Simple scaling suggests that the kinetic energy flux is considerably smaller. In geostrophic balance, the ratio of kinetic to geopotential energy flux is $\Delta K/\Delta\Phi \approx u^2/fuL \approx u/fL \approx 0.1$, where u is a typical wind speed at the tropopause, L is a characteristic length (a few 1000 km), and f is the Coriolis parameter.

Gierasch *et al.* (1986) have proposed an analogous circulation above 0.5 bars on Jupiter. We can estimate the boundary terms for the jovian circulation using vertical velocities from Gierasch *et al.* (1986) and West *et al.* (1992). The zonal jets have typical speeds of 40 m s^{-1}, which in geostrophic balance implies that the difference in geopotential energy (along isobars) between belts and zones is 3×10^4 m^2 s^{-2} (at 30° latitude, assuming the belt-zone spacing is 5000 km). Retrieved vertical velocities, of order $\omega = 6 \times 10^{-5}$ Pa s^{-1} at 270 mbar, suggest that upwelling occurs in regions of high Φ and downwelling in regions of low Φ; the resultant geopotential energy flux is ~0.08 W m^{-2}. In contrast, the mean kinetic energy is $\sim 2 \times 10^3$ m^2 s^2, implying a flux of order ~0.005 W m^{-2}. At the probe site's latitude of 6.5°N, the calculation gives geopotential and kinetic energy fluxes of 0.05 and 0.02 W m^{-2} (using $u = 100$ m s^{-1}), although the assumption of geostrophic balance is less likely to hold since the Rossby number is about 0.5.

2.3. *Comparison of Our Model with Other Proposed Models*

Two other proposed scenarios exist for depletion of volatiles and clouds at the probe site down to 20 bars. Guillot (1996, 1995) suggested that convection is inhibited at depths where water vapor (hence molecular mass) rises with pressure, and that the low volatiles measured by the probe might be a globally widespread condition. He hypothesized that the internal heat is transported upward by radiation or diffusive (oscillatory) convection (Turner 1973). We differ from Guillot's viewpoint in two respects. First, in the absence of a downdraft, small-scale mixing should transport volatiles upward across the stable layer to the condensation level. We feel that a downdraft is needed to counteract this mixing. Compensating updrafts must exist elsewhere; volatiles would not be depleted in those regions. Second, temperature differences between these (large-scale) updrafts and downdrafts could transport heat—we need not require radiation or diffusive convection to deliver the entire heat flux.

Engel *et al.* (1996) hypothesized that rapid subsidence inhibits upward transport of water vapor from Jupiter's

interior. They used a height and time dependent cloud model to calculate cloud densities as a function of the imposed large-scale subsidence rate; upward mixing of water was modeled as a diffusive process, with a diffusivity calculated from mixing length arguments. With no subsidence, the model produced clouds much thicker than those observed by Galileo; a subsidence rate of 1–2 m s^{-1} was needed to keep the model dry and free of clouds. (This velocity matches that predicted by mixing length theory for Jupiter.) The resultant downwelling time from the tropopause to the 10-bar level is about one day. This subsidence rate is fast enough to preclude radiative cooling of the downdraft.

In contrast to Engel *et al.*, we suggest that dryness at the probe site is maintained by a deep stable layer which inhibits convection from below. In the absence of subsidence, the stable layer will rise as volatiles are mixed upward by turbulence below the layer; subsidence is therefore still necessary to maintain the position of the stable layer in steady state. The required descent time is quite long, however, and is consistent with the radiative time constant. We can calculate the required subsidence rate as follows. Suppose that convective plumes from the deep atmosphere overshoot into the stable layer, entraining a small amount of the low-density air into the deep atmosphere. This process produces potential energy, which derives from the kinetic energy of the overshooting plumes. Assume the power per area converted from kinetic to potential energy is $P_{\rm conv}$. If a mass per area dp/g of low-density air is mixed down a distance h below the stable layer over a time dt, then the increase in potential energy per area is

$$\frac{\Delta T_{\rm v}}{T_{\rm v}} \frac{dp}{g} gh \sim P_{\rm conv}\, dt,$$

where $\Delta T_{\rm v}$ is the virtual temperature stability of the layer (relative to a dry adiabat) and $T_{\rm v}$ is the virtual temperature. The stable layer therefore migrates upward at a velocity (in pressure coordinates) of dp/dt given by

$$\frac{dp}{dt} = \frac{P_{\rm conv} T_{\rm v}}{\Delta T_{\rm v} h}.$$

The dry air must therefore subside at this rate for the position of the stable layer to be maintained. We estimate $P_{\rm conv}$ as follows. The internal heat flux at the equator is about 5 W m^{-2} (Ingersoll and Porco 1978). If the entire heat flux is convected and if we assume the convective motions are 20% efficient in producing kinetic energy (as would be expected from heat engine arguments if convection occurs over a scale height), then $P_{\rm conv} = 1$ W m^{-2}. We use $\Delta T_{\rm v} = 4$ K, comparable to the expected difference in virtual temperature between the upper troposphere and deep atmosphere for solar water abundance. Using $T_{\rm v} = 400$ K and $h = 60$ km (one scale height), we obtain a subsidence rate of 2×10^{-3} Pa s^{-1} necessary to keep the downdraft dry. The resulting descent time from the tropopause to 10 bars is 20 years. Even if we take $P_{\rm conv} = 5$ W m^{-2}, the descent time is 4 years, still long enough to allow radiative cooling of the downdraft.

The trade-wind inversion on Earth is maintained by processes similar to those suggested here (Betts 1973, Emanuel 1994). Because of the strong inversion, subsidence speeds of 0.005 m s^{-1} are sufficient to balance upward mixing of boundary layer air, despite the fact that boundary layer plumes *below* the inversion move at vertical speeds up to 1 m s^{-1} (e.g., Garratt 1992, p. 214).

3. PUZZLE II: THE PROBE WINDS

The winds obtained by Doppler tracking of the Galileo probe signal from the orbiter are shown in Fig. 3 (Atkinson *et al.* 1996, 1997). The preferred fit to the data yields zonal winds which are 90 m s^{-1} at the 0.5 bar ammonia cloud level, increasing to 180 m s^{-1} at 5 bars, and decreasing to 170 m s^{-1} below 15 bars. The 1-σ uncertainty is roughly 10 m s^{-1}, so the decrease in speed from 5 to 15 bars is

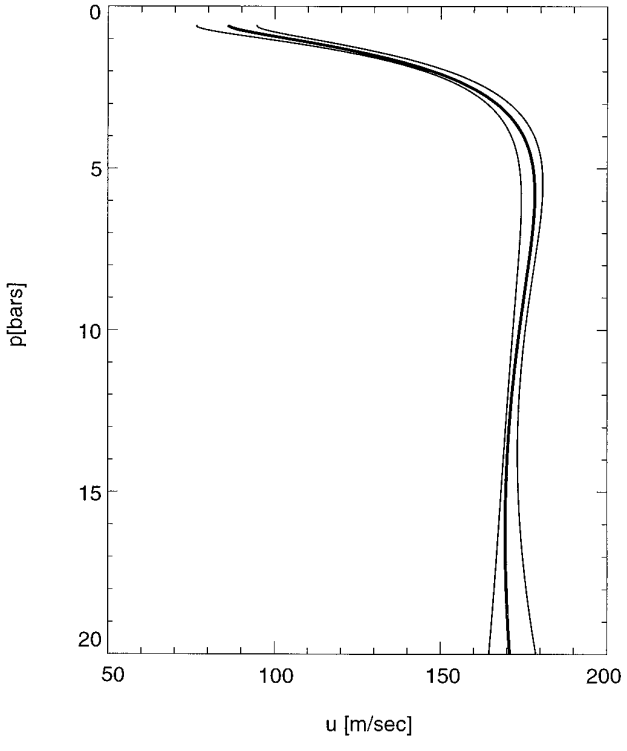

FIG. 3. Winds versus depth measured by Doppler tracking of Galileo probe signal from the orbiter (data from Atkinson *et al.* 1997). The thick curve is a nominal fit to data; thin curves denote the 1-σ error envelope.

valid to about 1-σ. The increase in winds from 0.5 to 5 bars appears robust and agrees with the winds obtained by Doppler tracking of the probe signal from the ground (Folkner *et al.* 1997). Further support for the winds is provided by probe acceleration data (Seiff *et al.* 1997a).

As described in the Introduction, these wind data are difficult to understand if geostrophic balance holds. When geostrophic and hydrostatic balance are combined, the well-known "thermal wind" relation results (Holton 1992, p. 73)

$$\left(\frac{\partial T_v}{\partial y}\right)_p = \frac{pfm_d}{k}\left(\frac{\partial u}{\partial p}\right)_y, \tag{4}$$

where T_v is virtual temperature, y is distance northward, p is pressure, m_d is the mass per molecule of "dry" air (free of ammonia, H_2S, and water), k is Boltzmann's constant, u is the zonal wind, $f = 2\Omega \sin \phi$ is the Coriolis parameter, Ω is the planetary rotation rate, and ϕ is latitude. The fact that $\partial u/\partial p > 0$ from 1 to 5 bars implies a stable layer in the hot spot in that layer, which seems inconsistent with a downwelling. However, at the probe's equatorial latitude of 6.5°N, the Coriolis force is relatively weak and the centripetal force due to curving flow trajectories becomes important. The thermal wind equation may therefore not hold, and another force balance must be used. In this section, we use the more general "gradient wind" force balance, a balance between pressure-gradient, Coriolis, and centripetal accelerations. We derive a range of possible vertical profiles of density in the hot spot as compared to that in the equatorial zone. The profiles are not unique because the new relation contains one poorly known parameter, the local radius of curvature of the winds at the probe site. (The profile obtained from geostrophic balance will be one such profile.) We then discuss the plausibility of each profile.

The gradient wind force balance in the meridional direction is

$$\frac{u^2}{R} + fu + \frac{\partial \Phi}{\partial y} = 0, \tag{5}$$

where R is the local radius of curvature of the wind trajectory (positive for trajectories curving to the left and negative for those curving to the right) and $\partial\Phi/\partial y$ is the gradient of geopotential Φ with northward distance y. (This equation holds for curving flow at the point where the flow is zonal.) Differentiating this equation with respect to pressure and using hydrostatic balance, we obtain the gradient-wind generalization of the thermal wind relation

$$\left(\frac{\partial T_v}{\partial y}\right)_p = \frac{pm_d}{k}\frac{\partial u}{\partial p}\left(\frac{2u}{R} + f\right). \tag{6}$$

No high resolution images exist for the probe entry hot spot, so R is unknown. We treat it as a free parameter. Galileo images of a different hot spot, however, show a large clockwise circulation southeast of the hot spot (Vasavada *et al.* 1997). These images suggest that negative (clockwise) values of R may be most appropriate.

When we substitute the known winds (Atkinson *et al.* 1996, 1997) into the equation using many values of R, we find that three types of $\partial T_v/\partial y$ profile exist. Examples of each are displayed in Fig. 4 (top row, (a)–(c)). The solid lines in the top panels result from using Atkinson *et al.*'s nominal wind profile (thick line in Fig. 3). To determine the approximate error in the $\partial T_v/\partial y$ curves, we constructed many hypothetical wind profiles which deviated from the nominal profile, yet still passed within the error envelope of the winds. The deviations were assumed to have a vertical wavelength of a few bars. The error bars in Fig. 4 (top row) delineate the range of $\partial T_v/\partial y$ values obtained from these hypothetical wind profiles. The profiles end at 12 bars because, at $p > 12$ bars, the uncertainty in $\partial T_v/\partial y$ becomes much greater than the mean value (this results directly from the increasing error in the winds from 12 to 20 bars; see Fig. 3).

The densities can also be expressed using the virtual potential temperature, defined as (Salby 1996, p. 124)

$$\theta_v \equiv T_v\left(\frac{p_0}{p}\right)^{\frac{\gamma-1}{\gamma}}, \tag{7}$$

where $p_0 = 1$ bar is a reference pressure and $\gamma = c_p/c_v$ is the ratio of specific heats at constant pressure and volume. Virtual potential temperature (which is equivalent to potential density) is more convenient than virtual temperature for expressing height variations of density because it accounts for the compressibility of air. When θ_v is constant with pressure, the profile is statically neutral to dry convection; when θ_v increases with height, the profile is stable to dry convection, and when θ_v decreases with height, the profile is unstable to dry convection.

The bottom row of Fig. 4 (panels (d)–(f)) shows the density profiles 2000 km north of the probe site, at the probe site, and 2000 km south of the probe site obtained by linearly extrapolating the dash–dot profiles of $\partial T_v/\partial y$ plotted in the top row. The densities are expressed using virtual potential temperature. The dash-dot profiles in panels (a)–(c) (top row) were chosen so that $\partial\theta_v/\partial y$ is independent of p wherever possible. When $\partial\theta_v/\partial y$ decreases with pressure ($\partial^2\theta_v/\partial y\partial p < 0$), the region south of the probe site must be taken as neutrally stable; the extrapolation is carried out toward the north, and all such regions contain some stability. (If we took the probe site or region to the north as neutrally stable, our extrapolation would force some regions to the south to be statically unstable, which

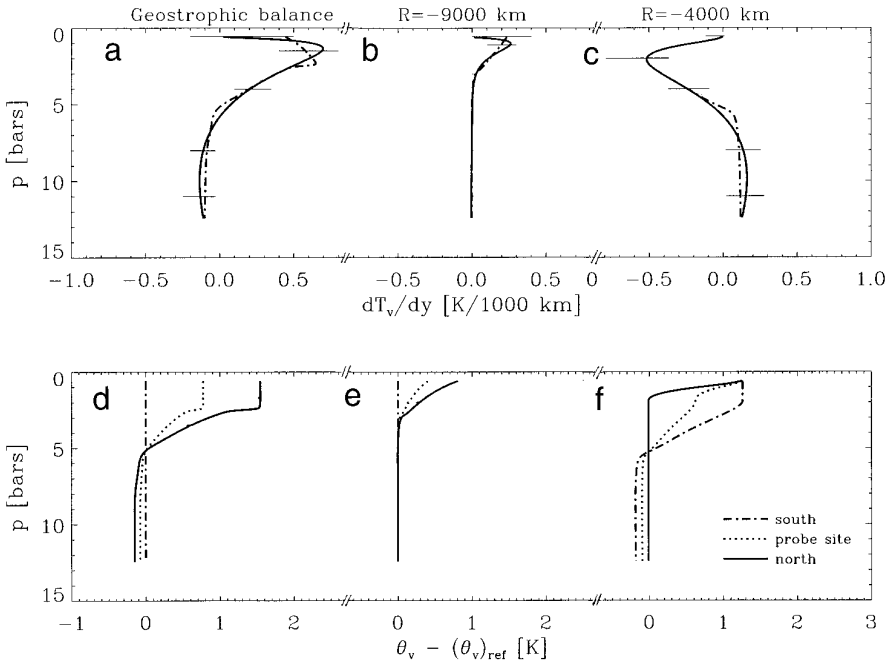

FIG. 4. (Top row) Profiles of $\partial T_v/\partial y$ versus pressure obtained from the winds assuming gradient wind balance for three cases: (a) geostrophic balance ($R \to \pm\infty$), (b) $R = -9000$ km, and (c) $R = -4000$ km. (Bottom row) θ_v versus pressure (relative to a constant reference Θ_v) obtained by linearly extrapolating the $\partial T_v/\partial y$ profiles (from the top row) 2000 km north and south of the probe site. Based on simple models of convection, the cases in the leftmost and middle columns are difficult to understand, but the rightmost makes sense. It is qualitatively similar to Fig. 2a.

is impossible.) When $\partial\theta_v/\partial y$ increases with pressure ($\partial^2\theta_v/\partial y\partial p > 0$), however, the region to the north is taken as neutrally stable, and the extrapolation is carried out toward the south. When $\partial^2\theta_v/\partial y\partial p$ changes sign, the region pinned to an adiabat switches from north to south of the probe site. The nominal $\partial T_v/\partial y$ profile (solid curve in panels (a)–(c)) requires several such switchings, leading to complicated interpretation. Most of the switchings, however, result from subtle variations in the nominal $u(p)$ which are far below the error bars; hence, these switchings contain no information. By using the dash–dot curves where $\partial\theta_v/\partial y$ is independent of pressure wherever possible, we limit the number of switchings to those *required* by the data.

Consider the first type of profile, shown on the left for geostrophic balance ($R \to \pm\infty$); qualitatively similar profiles hold for negative (clockwise) values of R exceeding 12,000 km in magnitude or for any positive (counterclockwise) value of R. Here, $\partial T_v/\partial y$ is positive from 1 to 5 bars and (marginally) negative from 5 to 12 bars. This implies that the hot spot (to the north of the probe site) is *less dense* (greater T_v) from 1 to 5 bars than the equatorial zone (south of the probe site). The hot spot is denser than the equatorial zone below 5 bars, however. This is seen in the virtual potential temperature profiles in Fig. 4d; the profiles were constructed by assuming the region to the south is dry adiabatic (i.e., neutrally stable). (We could have chosen the region to the south to be stable, in which case the hot spot would be even more stable. Similarly, if we chose the hot spot or the probe site to be neutral, the region to the south would be unstable to dry convection, which is impossible. Figure 4d shows the *minimum* stability inside the hot spot and at the probe site consistent with the physical requirement that no region within 2000 km of the probe site be unstable. This is probably an appropriate distance to use because it is comparable to the size of atmospheric features and therefore to the maximum range over which $\partial T_v/\partial y$ can be reliably extrapolated.) The region to the north shows a strong stable layer from 2 to 5 bars (θ_v decreasing with depth). This results directly from the fact that $\partial u/\partial p$ decreases strongly from 1 to 5 bars, which is a robust feature in the wind data. The greater density in the hot spot below 5 bars results from the decrease in wind speed from 5 to 12 bars, and is therefore robust to about 1-σ.

The results in Fig. 4d violate our expectations. First, because of the low radiative flux divergence below 2 bars (Sromovsky *et al.* 1996, 1997), downwellings should follow dry adiabats there. Although a stable layer above 5 bars can result from moist convective upwelling with a solar water abundance, this is not consistent with downwelling in the hot spot. Second, because Voyager data suggest upwelling near the equator (Gierasch *et al.* 1986), we might expect the region south of the probe site to contain a stable layer resulting from moist upwelling. However, the region

south of the probe site is less stable than the probe site itself (Fig. 4d), which is nearly dry adiabatic (Seiff *et al.* 1997b); the equatorial zone region south of the probe site must therefore be even closer to dry adiabatic. The inferred profiles are difficult to understand because they predict that the virtual temperature between downdrafts and updrafts decreases with depth, contrary to expectation. Third, the dry downwelling should be less dense below 5 bars, while Fig. 4d suggests the reverse. Therefore, while the geostrophic case plotted in Figs. 4a and 4d is consistent with the winds, it cannot be reconciled with our expectations about how and where convection occurs.

Consider instead a second type of profile, shown in the middle column of Fig. 4 for $R = -9000$ km, and valid for any negative R (clockwise trajectory) with magnitude between 8000 and 12,000 km. This profile suggests that $\partial T_v/\partial y$ is positive from 0.5 to 3 bars and zero below 3 bars. Profiles north and south of the probe site therefore have equal densities (along isobars) below 3 bars, but above 3 bars the hot spot is less dense. The hot spot is therefore *stable* above 3 bars (Fig. 4e). (Below 3–4 bars, the virtual temperature gradient is zero because the pressure-gradient force has dropped out; the resultant balance—inertial balance—is between Coriolis and centripetal forces. For a given R, such balance occurs only for a particular value of u. Inertial balance approximately holds at all heights below 3 bars because the winds vary only slightly with depth there.) Although possible, this scenario is also difficult to reconcile with simple convection models. The stable layer cannot result from moist convective upwelling since water can only produce significant stable layers near 5 bars; the stability resulting from H_2S condensation is too small to match that required here. Radiative cooling and subsidence could produce a stable layer. This qualitatively matches the net flux radiometer observations that substantial cooling occurs at pressures less than 2–3 bars, with little cooling at greater pressures (Sromovsky *et al.* 1996, 1997). However, Fig. 4e suggests that the stability in the hot spot equals that in the equatorial zone at $p > 3$ bars. If the equatorial zone were an upwelling, it should be stable from 2 to 6 bars (Fig. 2). The hot spot would then also contain a stable layer from 2 to 6 bars, which is difficult to understand.

The third scenario is shown in Fig. 4c for $R = -4000$ km; a qualitatively similar profile results for any negative values of R with magnitude less than 6000 km. Here, $\partial T_v/\partial y$ is negative from 1 to 5 bars and (marginally) positive from 5 to 12 bars; it is similar in magnitude but opposite in sign to the first case we described (left column of Fig. 4). Therefore, this profile suggests just the reverse: that from 1 to 5 bars, the region to the south is *less dense* than the region to the north of the probe site; below 5 bars, the region to the south is denser than that to the north. Virtual potential temperature profiles are shown in Fig. 4f, assuming the region 2000 km north of the probe site is dry adiabatic. (Above 1.5 bars, the region *south* of the probe site is assumed dry adiabatic.)

These ideas fit our expectations: they suggest that regions to the south are *stable* from 2 to 6 bars, consistent with moist adiabatic upwellings, and that the regions to the north are dry adiabatic below 1.5 bars. Further, they suggest that the hot spot is less dense from 5 to 12 bars (though again this result is robust to only 1-σ), as required to prevent mixing of volatiles from below. As before, the stable layer above 6 bars results from the major change in $\partial u/\partial p$ between 1 and 6 bars, a robust feature in the data. The pressure at the base of this stable layer results directly from the wind data and is *independent* of any assumptions about moist convection. Nevertheless, it agrees well with that predicted for moist adiabatic upwellings containing a water abundance of 1–2 times solar (Atreya and Romani 1985). (The magnitude of these density differences is poorly constrained. All values of -6000 km $< R < 0$ yield $\partial T_v/\partial y$ profiles *qualitatively* similar to that in Fig. 4c, including the stable layer above 6 bars and the sign of the density differences at all levels. The exact *magnitude* of $\partial T_v/\partial y$ is sensitive to R, however.) Interestingly, the θ_v profiles show a stable layer above 1.5 bars in the hot spot. This feature, which appears to be robust, is suggestive of radiative cooling in the downwelling above 1.5 bars; further, it implies that the hot spot may be less dense than the equatorial zone above 0.5 bars, as suggested in groundbased infrared data (Orton *et al.* 1996).

In summary, based on simple notions of how convection should operate, we favor the rightmost column of Fig. 4. The negative values of R required for this scenario are in qualitative agreement with the fact that a clockwise circulation was seen south of a hot spot in Galileo images, although the observed radius of curvature may be greater than 6000 km as measured in System III (Vasavada *et al.* 1997).

All values of R require the probe site to be slightly stable above a few bars depth. If the profiles had been calculated assuming the probe site were neutrally stable, then some regions away from the probe site would be unstable, which is impossible. The required stability at the probe site scales with the latitude range over which $\partial T_v/\partial y$ is extrapolated; for 2000-km extrapolation in either direction, the required stability is $\sim$1 K (Figs. 4d–4f). Although the probe temperature measurements suggest a dry adiabatic profile (Seiff *et al.* 1997b), the uncertainty is about 1 K. The stable layer which is required for a consistent explanation of the winds may therefore be consistent with the temperature data.

The $\sim$1 K stability quoted above implies a Richardson number of about 0.5 between the ammonia cloud top and 5 bars.

In the scenarios above, we assumed that R was constant

with depth. If R varies with depth, the number of possibilities multiplies by many-fold. We give one example. Suppose the hot spot is less dense than the equatorial zone at all depths (as in Fig. 2b) and that the probe entered the boundary between the two regions. $-\partial\Phi/\partial y$ (a positive quantity) then increases with depth from 0.5 to 20 bars. From 0.5 to 5 bars, geostrophic balance holds, so the increasing $u(p)$ allows the balance $fu = -\partial\Phi/\partial y$. At $p > 5$ bars, the wind is constant with depth, so the increasing $-\partial\Phi/\partial y$ must be balanced by u^2/R. This requires positive R with decreases with depth. The interpretation is as follows. The deep hot spot is a cyclonic vortex at the southern edge of the north equatorial belt; the probe fell into the south edge of the vortex. The top of the vortex is at 5 bars. Above that there is no vortex. This model explains the absence of a vortex in Galileo images of a hot spot (Vasavada *et al.* 1997) and may also explain the long lifetime of hot spots (Ortiz *et al.* 1997)—hot spots are all underlain by long-lived deep vortices which do not penetrate to the cloud level. If the winds are truly zonal at the probe site, however, models such as this are improbable: the wind vectors are unlikely to be parallel at all depths if the flow curvature varies with depth as well. However, Atkinson *et al.* (1997) *assumed* zonality in deriving their wind profile. Although tracking of the probe signal from the ground seems to corroborate this assumption from 1 to 5 bars (Folkner *et al.* 1997), substantial uncertainties exist, and their data place no constraints on the wind at $p > 5$ bars. Further, while Seiff *et al.*'s (1997a) analysis of probe accelerometer measurements have yielded a wind profile in qualitative agreement with that of Atkinson *et al.*, they assumed zonality as well. It is possible that these data would allow nonzonal winds whose direction varied with depth; if so, models with height-variable R become more plausible.

4. PUZZLE III: INTRODUCING VOLATILES AT DIFFERENT HEIGHTS

As shown in Fig. 1, analysis of the attenuation of the probe radio signal suggests that ammonia increased rapidly with depth from 1 to 8 bars, reaching a plateau at $p > 8$ bars (Folkner *et al.* 1998). Further, according to data taken from the Galileo probe's mass spectrometer, H_2S surged from 0.3 times solar at 8.6 bars to solar by 9.6 bars, tentatively leveling off to 2.7 times solar at 16 bars (Niemann *et al.* 1996, 1997). Water, however, was less than 3% and ~30% solar at 12 and 19 bars, respectively (Niemann *et al.* 1997). These measurements are puzzling. They suggest that the observed volatiles were not introduced into the downdraft by *vertical* mixing, since moist plumes rising from below should have the deep, constant ratios of the NH_3, H_2S, and water mole fractions, and mixing of these plumes into the dry downdraft would not change these ratios.

Here, we present two plausible mechanisms for producing the observed pattern of increasing volatiles with depth. An important clue is that the order in which the volatiles rise with depth mimics that predicted by equilibrium condensation models (Weidenschilling and Lewis 1973) but occurs at much greater pressures (Fig. 1).

4.1. Lateral Mixing

First, as suggested by Atreya *et al.* (1997), volatiles could be introduced into the downdraft by *lateral* mixing. The volatiles from 1 to 8 bars at the probe site would have originated above the NH_3 lifting condensation level (at perhaps 0.6 bars for solar abundances) in an adjacent region, since this is the expected pressure range where ammonia increases strongly with depth while H_2S and water remain low (Fig. 1, right panel). Similarly, the increase in H_2S from 9 to 16 bars would occur because air originating near the NH_4SH condensation level (near 2 bars) elsewhere mixed downward to 9–16 bars at the probe site. The relative absence of H_2S above 9 bars would be explained because any material mixed to pressures less than 9 bars at the probe site would have originated above ~1 bar in the source region, where H_2S is absent. The obvious mechanism is that the mixed air follows isopycnals, or surfaces of constant virtual potential temperature (Eq. (7)). Physically, this simply means that when parcels move from one stable air column to another, they maintain their position of neutral buoyancy. If the new air column is less dense than the old column, the parcel's height of neutral buoyancy will decrease as it moves, so the mixed air will sink. Conversely, if the new column is denser, the mixed air will rise as it enters the new column. Mixing is observed to follow isopycnals in Earth's atmosphere and oceans when diabatic forcing is weak (e.g., Holton *et al.* 1995).

In Fig. 5, we illustrate the mixing process for two situations, corresponding to the density profiles in Figs. 2a and 2b. In Fig. 5a (top panels), the hot spot is denser than the surroundings from 1 to 5 bars and less dense below 5 bars, as would occur if the downwelling undergoes radiative cooling as it descends into the hot spot. Near the 5-bar level, the density in the hot spot is the same as in the surroundings; this corresponds to a horizontal isopycnal (surface of constant θ_v). Above 5 bars, the isopycnals bow upward within the hot spot because it is denser than the surroundings, while below 5 bars, they bow downward. This scenario cannot explain the observations. It predicts that H_2S should be present in the hot spot at all heights below 2 bars, contrary to observation; water should be abundant everywhere below 5 bars. Ammonia should be constant below 0.6 bars, in disagreement with observation (Folkner *et al.* 1998).

Figure 5b (bottom panels) shows the second scenario. Here, the hot spot is less dense than the surroundings at all heights below 0.5 bars; this corresponds to the situation

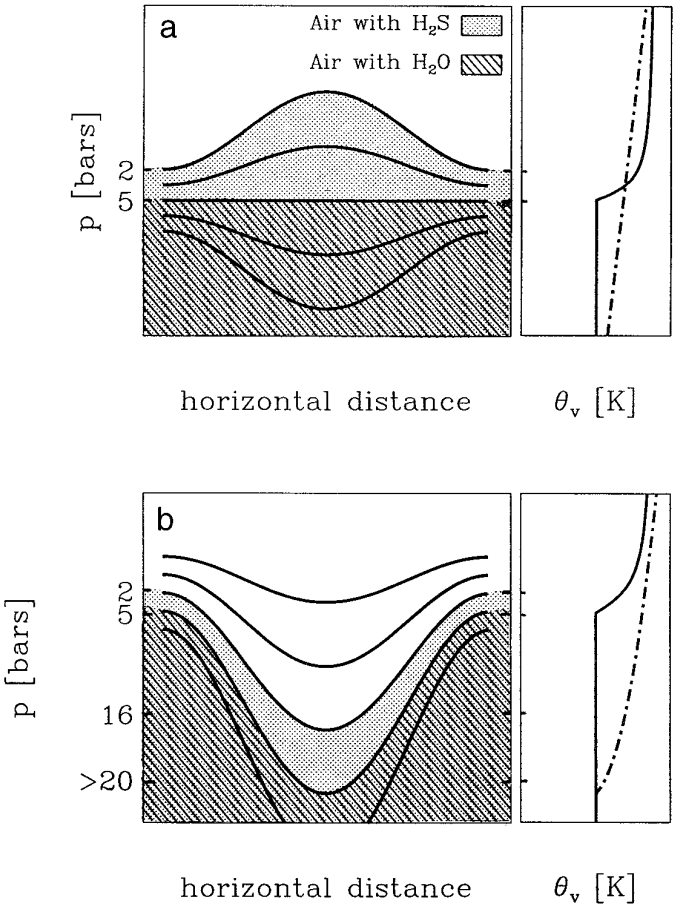

FIG. 5. Two possible scenarios for mixing volatiles into the downdraft, assuming mixing along isopycnals. Left panels depict isopycnals (solid lines) vs pressure and horizontal distance; the hot spot is assumed to span the middle half of the horizontal axis. Right panels show the assumed virtual potential temperatures. The dash–dot and solid curves are the profiles in the hot spot and surroundings, respectively. (a) From 1 to 5 bars the hot spot is assumed denser than the surroundings; for $p > 5$ bars, it is less dense (as in Fig. 2a). This cannot explain the data shown in Fig. 1. (b) The hot spot is assumed less dense for all $p > 0.5$ bars (as in Fig. 2b). This readily explains the observed profiles of NH_3, H_2S, and H_2O shown in Fig. 1.

where the upwelling air radiatively warms before descending into the hot spot (or where the circulation time is so rapid that no radiative warming or cooling can occur). In this scenario, the isopycnals bow downward inside the hot spot at all heights. Therefore, volatiles at all heights move downward as they enter the hot spot. This scenario readily explains the mass spectrometer and signal attenuation observations compiled in Fig. 1. Air parcels containing traces of H_2S, which begin at perhaps 1 bar, move to 9 bars at the probe site. Air at the 2 bar NH_4SH lifting condensation level moves to 16 bars at the probe site. This explains why the H_2S mole fraction was constant below 16 bars. Material originating at 5 bars mixes to depths below 20 bars; this explains why the probe measured a water mole fraction which was still increasing at 20 bars. This model therefore provides a natural explanation for why the downdraft remains dry despite the fact that horizontal mixing appears to be very vigorous on Jupiter. (Possibly, dissipative processes could cause a small component of horizontal mixing *across* isopycnals. Subsidence would then be required to maintain the scenario shown in Fig. 5b in steady state. This is analogous to the balance between subsidence and mixing described in Section 2.3.)

If lateral mixing is to explain the observed pattern of volatiles, therefore, an important implication results: the dry downdraft is *less dense* than the volatile source region at all depths below 0.5 bars. (Because mixing along isopycnals conserves θ_v—a measure of density—such mixing cannot affect the density structure. The low density must be independently created by another mechanism, perhaps that suggested in Section 2.) If the volatile source region is south of the probe site, this contradicts our favored interpretation of the probe winds, which suggests that (from 1 to 5 bars) the hot spot is denser than the region directly south of the probe site. Possibly, the volatiles mixed into the probe site originated in a different region with a greater density.

4.2. *Column Stretching*

Alternatively, the observed profiles might result from column stretching in complete absence of lateral mixing. In this scenario, the air at the probe site would have begun with ammonia decreasing above 0.6 bars, H_2S decreasing above 2 bars, and water decreasing above 5 bars, as predicted by thermochemical models (Weidenschilling and Lewis 1973; see Fig. 1). Suppose that the top of the air column were maintained at roughly the same height, while the bottom of the column moved downward. As the column stretched, the *relative* location of all parcels within the column would be fixed. The increase in NH_3 from 1 to 8 bars would then be the signature of a "fossil" NH_3 lifting condensation level which originated at 0.6 bars but was pushed to 8 bars during the stretching process; similarly, the NH_4SH lifting condensation level would be pushed from 2 to 16 bars. The original water lifting condensation level near 5 bars would be pushed even deeper, explaining the observation that H_2S increased before water.

This scenario provides a natural explanation for the nearly dry adiabatic conditions at the probe site. A moist adiabat associated with three times solar H_2S produces 0.1 K of warming relative to a dry adiabat (Atreya and Romani 1985). We therefore expect 0.1 K of (temperature) stability between 9 and 16 bars at the probe site, consistent with observation. Although condensation of water yields warming of 2 K for solar abundance, this stability may have been positioned somewhat below 20 bars.

Stretching might occur in a manner analogous to flow over mountains on Earth. On Jupiter, the topography might consist of a deep ($p > 20$ bar) isopycnal surface which varies in height from place to place. As the air column moved over the variable isopycnal, it would stretch and contract. This speculation might be testable by measuring the vorticity ζ along air trajectories in Galileo images. Parcels tend to maintain constant values of potential vorticity, defined (in the shallow water context) as $(\zeta + f)/h$, where f is the Coriolis parameter and h is the height of the column. If air columns elongated as they moved over the hot spot, the value of ζ would change along streamlines.

This scenario qualitatively matches Galileo orbiter observations that air flowed into a hot spot at 30 m s^{-1} from the southwest (Vasavada *et al.* 1997). If the column elongated and contracted as it entered and exited the hot spot, the time between elongation and contraction would be 1–2 days.

This simple model predicts that the dry downdraft is less dense than the initial (prestretched) profile at all pressures. If the initial, prestretched density profile is the same as that in the regions surrounding the hot spot, then the isopycnals must bow downward in the hot spot, as in Fig. 5b.

5. WHAT DO THE DATA SAY ABOUT THE FORCING?

In Section 2 we proposed that the hot spot circulation is thermally indirect below 5 bars. For this hypothesis to be reasonable, the energy liberated by the atmospheric heat engine must be great enough to push dry air to 10 bars or deeper. In this section, we address this issue by using available data to tentatively evaluate the magnitude and nature of the forcing. Because of the paucity of data, we cannot directly evaluate any of the terms in Eq. (3). However, we do have limited information on the vertical profiles of density from 0.5 to 20 bars in the hot spot relative to its surroundings. We therefore may be able to find the column integrated density in the hot spot and compare it to that in the surroundings. This comparison will allow us to determine whether the vertical flux of geopotential energy is sufficient to drive the indirect motions.

To attack this problem, we recast the kinetic energy Eq. (3) from Section 2 into another form. Averaging in time and assuming the circulation consists of a mean circulation followed by all parcels (an approach used on Earth by Renno and Ingersoll (1995)), Eq. (3) becomes

$$\dot{M} \int \frac{k}{m_d} (T_v|_{up} - T_v|_{down})\, d \ln p = \dot{M} \int \left(\frac{1}{\rho_{up}} - \frac{1}{\rho_{down}} \right) dp = \overline{F}_{bot} + \overline{F}_{top} + \overline{F}_{sides} - \overline{D}, \quad (8)$$

where the overbar denotes time average and F_{bot}, F_{top}, and F_{sides} are the sums of kinetic and geopotential energy flux at the bottom, top, and side boundaries. $\dot{M}$ is the mass per time transported through isobars in the updrafts and downdrafts divided by the horizontal area of the domain, ρ_{up} is the density in locations where a moving parcel's pressure decreases with time, and ρ_{down} is the density in regions where pressure increases with time.

Although we cannot evaluate $\dot{M}$, $\overline{F}_{bot}$, $\overline{F}_{sides}$, or D, the data provide constraints on $\int \rho_{up}^{-1} - \rho_{down}^{-1}\, dp$. If this integral is positive, the *column integrated* motion is thermally direct; the direct motion from 1 to 5 bars provides sufficient geopotential energy flux to drive the indirect circulation at deeper levels. If negative, the column integrated motion is thermally indirect and other forcing is required.

Three forms of data have implications for the density of the hot spot relative to the surroundings. These are (1) a comparison of Voyager occultation and Galileo probe temperature data, (2) the interpretation of the probe winds presented in Section 3, and (3) the interpretation of the mass spectrometer data presented in Section 4. We consider each in turn.

5.1. Temperature Data

The Voyager radio occultation experiment measured temperatures to the 1-bar level at two latitudes, one at the equator and another at 13°S in the south equatorial belt (Lindal *et al.* 1981). When corrected for the new He/H_2 value from Galileo (Niemann *et al.* 1996, von Zahn *et al.* 1996), the data imply temperatures of 169 K at 1 bar. The 5 K uncertainty quoted by Lindal *et al.* includes error in both the data themselves and in the assumed helium abundance. For a known helium abundance, the error in temperature is probably about half this value (Conrath *et al.* 1984). In contrast, the Galileo probe measured a temperature of 166 ± 1 K at 1 bar (Seiff *et al.* 1997b). Thus, the hot spot appears to be colder at 1 bar than the regions sampled by Voyager.

If downwelling occurs in the hot spot and upwelling occurs at the equator (as suggested by high cloud abundance and cold temperatures above the clouds there, Gierasch *et al.* 1986, Carlson *et al.* 1994), the temperatures listed above suggest that the motion at 1 bar is thermally direct. We wish to determine whether this thermally direct motion provides enough energy to force dry air to 10–20 bars. To do so, we assume that the external energy fluxes (minus dissipation) are negligible, so that the sole energy source is the direct loop in Fig. 2a. Eq. (8) then becomes

$$\int_{p_{bot}}^{p_{top}} \frac{1}{\rho_{up}}\, dp = \int_{p_{bot}}^{p_{top}} \frac{1}{\rho_{down}}\, dp \quad (9)$$

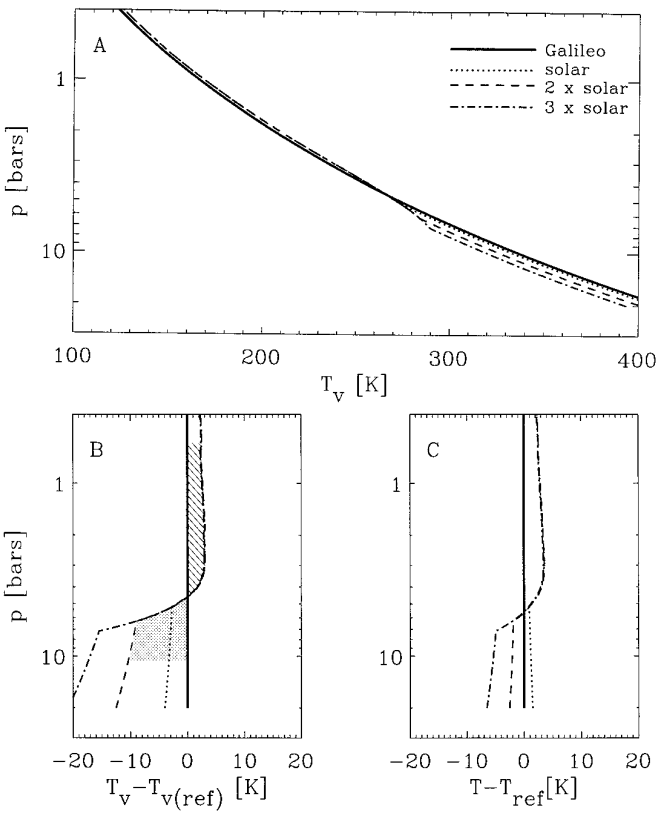

FIG. 6. (a) Virtual temperature vs log p for a dry adiabat representing the Galileo probe data (solid line), and for several moist adiabats with various assumed deep water abundances. All the moist adiabats pass through 169 K at 1 bar, as measured by the Voyager occultation. (b) The same, but with the dry adiabat subtracted off. The zero-dissipation/forcing condition requires that the area between the probe data and a given moist adiabat is zero, implying for the 2 times solar case that the hatched area equals the stippled area. This sets the depth at the base of the downdraft. (c) Temperature vs log p, with the Galileo dry adiabat subtracted off.

We now use Eq. (9) to estimate the depth of the dry downdraft. Combining data from the Galileo probe's atmospheric structure experiment (Seiff *et al.* 1996, 1997) with that from the Voyager radio occultation experiment (Lindal *et al.* 1981) allows us to estimate the two terms in the equation. We use the probe data for the downdraft. We use the Voyager data for the updraft; we extrapolate downward with a moist adiabat. When the saturation water vapor mixing ratio exceeds an assumed deep value (which occurs at 5, 6, or 7 bars for 1, 2, or 3 times solar, respectively), we continue the extrapolation as a dry adiabat (as occurs in Fig. 2).

Figure 6a illustrates the virtual temperature vs log p for the Galileo data (solid line) and for several moist adiabats, all of which pass through 169 K at 1 bar (other curves). The various moist adiabats assume different deep water abundances, from 1.0 to 3.0 times solar. Figure 6b illustrates the same curves, but with the Galileo dry adiabat subtracted off. When interpreted as a single thermodynamic cycle (up along a moist adiabat and down along the dry adiabat), the area of the cycle is proportional to work done. Our assumption of no dissipation and no forcing implies no net work, so that the "positive" area (hatched) cancels out the "negative" area (stippled for the 2 times solar case). For a given moist adiabat, this specifies the depth to which the "negative" area can extend; i.e., it sets the depth of the dry downdraft. (We assume the downdraft has 20% solar water abundance above this depth, Niemann *et al.* 1996.) For 1, 2, or 3 times solar water, the downdraft extends to 30, 11, or 9 bars, respectively. A virtual temperature stability of several K is predicted at the base of the dry downdraft.

Therefore, *in the absence of external mechanical energy fluxes*, the thermally direct motion from 1 to 5 bars can provide enough energy to force dry air to 10–30 bars, as observed. (If kinetic energy or pressure forces created elsewhere do additional work on the indirect circulation, the dry downdraft could extend even deeper.)

Because the scenario here requires radiative cooling, we expect the downwelling time to be of order years. If gradual upwelling occurs over half the area, the upwelling and downwelling times could be comparable. If upwelling occurs in isolated thunderstorms occupying a small fractional area (as on Earth), the upwelling time could be as short as hours.

5.2. *Interpretation of Wind Data*

Our favored interpretation of the probe winds (Fig. 4, rightmost column) suggests that the hot spot is denser than the equatorial zone from 1 to 5 bars, but less dense than the equatorial zone below 5 bars. Again, this suggests a thermally direct circulation overlying the indirect circulation. We use the solid and dash–dot lines from Fig. 4f as the downdraft and updraft, respectively. We find that the integral in Eq. (8) (taken from 0.5 to 12 bars) is positive, so that the direct circulation releases more energy than the indirect circulation (from 5 to 12 bars) absorbs. If we extrapolate these curves downward we find that the depth at which the energy integrals balance—and hence the maximum depth of a dry downdraft powered only by the direct loop from 1 to 5 bars—is 1000 bars. (If only half the energy released in the direct loop goes into the indirect motion, the maximum depth is 100 bars.) The reason this depth is so much larger than that obtained from the temperature data is that according to the wind data, the virtual temperature in the downdraft is only 0.3 K greater than that in the updraft at 10 bars. In contrast, the virtual temperature difference obtained from the temperature data (at 10 bars) is 4, 11, and 17 K for 1, 2, and 3 times solar water abundance, respectively.

These results suggest that the energy released in the thermally direct part of the circulation from 1 to 5 bars is

sufficient to push dry air to depth comparable to, perhaps far exceeding, those sampled by the probe. Thus, if (1) the hot spot is denser than the surroundings (from 1 to 5 bars) as suggested by wind and temperature data, and (2) this density contrast is indicative of updraft–downdraft differences, then the hot-spot circulation may be "self-driving," requiring no energy input from other regions on Jupiter.

5.3. Interpretation of Mass Spectrometer Data

If lateral mixing is to explain the increase in H_2S at lower pressures than water, then the hot spot must be less dense at all heights from 0.5 bars to the base of the dry downdraft; this may be true for stretching as well. This suggests that external forcing of the downdraft is required (the integral in Eq. (8) is negative). Here, we estimate the forcing such dry downdrafts might require and compare it to that made available by the atmosphere.

The power per area absorbed by indirect circulations can be estimated from Eq. (8). Suppose the dry downdrafts have a virtual temperature ΔT_v greater than that of the updrafts. The vertical mass flux in the dry downdrafts is $\dot{M} \approx \omega/g$, where $\omega = dp/dt$ is the vertical velocity in pressure coordinates. The mean power per area absorbed by the dry downdrafts is (from Eq. (8)) $\Delta T_v\ k\ \ln(p_{bot}/p_{top})\ \omega/(gm_d)$. We assume the dry downdrafts extend from the ammonia cloud level ($p_{top} = 0.5$ bars) to a lower pressure $p_{bot} = 20$ bars, with $\omega = 6 \times 10^{-5}$ Pa s^{-1} as obtained from retrievals at 270 mbar (West *et al.* 1992). We use $\Delta T_v = 3$ K, which corresponds to the stability difference between updrafts and downdrafts below a few bars if the water abundance is near solar and little radiative cooling occurs near cloud top. The mean power per area absorbed by the indirect circulations is then about 0.1 W m^{-2}. If we instead use $\omega = 2 \times 10^{-3}$ Pa s^{-1}, as may be required to balance the upward mixing of volatiles (Section 2.3), the power per area is 3 W m^{-2}. (This result assumes dry downdrafts cover essentially half the planet; if they are confined to local areas, the power per area would be lower.) These values are substantially less than Jupiter's 14 W m^{-2} mean heat flux and could be comparable to the generation of large scale energy by atmospheric convection. Existence of such indirect circulations is thus energetically reasonable.

6. DISCUSSION

The Galileo probe measured substantially depleted volatiles to 12 bars or deeper, suggesting that the probe entered a dry downdraft. We provided possible resolutions to three problems raised by Galileo probe data. To explain the dryness below the condensation level, we proposed that the downdraft is part of a thermally indirect circulation, operating as a heat engine in reverse. This suppresses convection from below and keeps the downdraft dry. Available data tentatively suggest that this circulation is energetically reasonable. Next, to explain the Galileo probe winds, we invoked gradient wind balance to calculate latitudinal gradients of density versus depth at the probe site. A range of profiles is possible, depending on the radius of curvature of the winds. Finally, the probe found that NH_3, H_2S, and water increased with depth at different rates (Fig. 1). We suggested that this signature results from either (1) lateral mixing along isopycnals, or (2) stretching of the air column down from $p < 0.5$ bars.

Some aspects of our different models are consistent with both external data and each other. Consider first our favored interpretation of probe winds. This interpretation suggests that for $p > 5$ bars, the hot spot is less dense than the equatorial zone—exactly as postulated to keep the downdraft dry (compare Fig. 4f with the diagram in Fig. 2a). Further, this scenario requires a counterclockwise circulation south of the hot spot; such a circulation pattern was seen in Galileo images for another hot spot (Vasavada *et al.* 1997). Finally, it suggests a stable layer in the hot spot above 1.5 bars. This stable region could allow the hot spot to be less dense than the equatorial zone for $p < 0.5$ bars, in accord with Voyager IRIS (Gierasch *et al.* 1986) and groundbased infrared (Orton *et al.* 1996) data.

The suggestion that the probe site is underlain by a stable layer (necessary to keep the downdraft dry) has both direct and indirect observational support. The temperature and mass spectrometer data together suggest that the probe site was statically stable below 12 bars, since temperature was dry adiabatic and molecular weight increased with depth. (Plumes rising from below would therefore have the same temperature as their surroundings but would have a greater molecular weight and hence density, so they would be inhibited from rising.) If water increased to solar below 20 bars, for example, the virtual temperature stability would be 3 K. Further, the fact that NH_3, H_2S, and water increased separately implies that the observed volatiles were not introduced into the downdraft by vertical convection from below. This is consistent with existence of a stable layer inhibiting such convection.

On the other hand, there appears to be a major inconsistency between our favored explanations for the wind and mass spectrometer data. Our favored interpretation of the winds (Fig. 4, rightmost column) suggests that from 1 to 5 bars, the hot spot (north of the probe site) is denser than the equatorial zone (south of the probe site). If lateral mixing is to explain the increase of volatiles at different heights, however, the hot spot must be less dense from 1 to 5 bars than the source region of the volatiles. If column stretching is to explain the increasing pattern of volatiles, then from 1 to 5 bars the hot spot should be less dense than the original (prestretched) column over this same height range. (This occurs because θ_v increases with height so that the stretching process increases θ_v at a given pressure.) In either case, if the region south of the hot spot has the same density structure as either the source region of the volatiles or the prestretched downdraft, then from

1 to 5 bars the hot spot must be less dense than the region to the south—in contradiction with our favored wind interpretation.

There are several possible resolutions to this inconsistency. The most likely explanation is that the region surrounding the hot spot is horizontally heterogeneous. If column stretching explains the volatile distribution, perhaps the original prestretched column was denser than that south of the probe site. Upon stretching, the hot spot would remain denser (from 1 to 5 bars) than the region to the south; this would reconcile the wind and mass spectrometer analyses. Or, if mixing explains the volatile distribution, perhaps the volatiles in the hot spot originated in a region denser than that directly south of the probe site. This would allow the 1–5 bar region at the probe site to be denser than that directly south of the probe site (as suggested by the winds), yet less dense than the source region for the volatiles (as suggested by the mass spectrometer data). Another possibility is that our favored interpretation of the winds is incorrect; perhaps another scenario in Fig. 4 applies, the radius of curvature varies with depth, or gradient wind balance does not hold. Unfortunately, all of these possibilities are ad hoc and prevent us from achieving a satisfying synthesis of the Galileo data.

The clouds observed by the probe further complicate attempts to form a coherent picture. The nephelometer and net flux radiometer detected a cloud near 1.4 bars and possibly another above 0.5 bars, but no 5-bar water cloud (Ragent *et al.* 1996, 1997, Sromovsky *et al.* 1996, 1997). The simplest explanation is that the 0.5- and 1.4-bar clouds (presumed to be ammonia and NH_4SH) result from upward mixing of ammonia and H_2S vapor into the downdraft, as shown in Fig. 5a; the sharp base of the 1.4-bar cloud would then be the NH_4SH-lifting condensation level. As observed, Fig. 5a also predicts that no water cloud would form because water is not mixed upward as it enters the hot spot. As described in Section 4, however, Fig. 5a cannot explain the mass spectrometer and probe signal attenuation results from Fig. 1. The cloud and mass spectrometer/signal attenuation data might be reconciled if an upper tropospheric cloud were mixed or advected downward along isopycnals to 1.4 bars (consistent with Fig. 5b). This is unlikely, however. To explain the mass spectrometer/signal attenuation data, the isopycnals in Fig. 5b must bow downward by about 80 km, while the observed cloud was only ~5–10 km thick. Reconciling the data sets therefore requires the cloud to have existed at just the right pressure in the upper troposphere, so that when advected 80 km down, it ended up exactly at the lifting condensation level (as required to explain the cloud's sharp base). Because cloud heights may follow isopycnals if the particle fall times are less than the cloud advection times, observations of cloud base pressures from Galileo NIMS or ground-based infrared data may help resolve this dilemma (e.g., Stewart *et al.* 1997).

New observations and modeling may help resolve the inconsistencies. Continued infrared and visible imaging observations from Galileo, Cassini, and the ground could clarify the extent to which dry regions are confined to hot spots, whether hot spots are coherent structures or waves propagating relative to the flow, and whether convergence (hence downwelling) occurs at hot spots (Vasavada *et al.* 1997). The answers may help us decide between the models presented here. High-resolution imaging from Galileo and Cassini may constrain the radii of curvature likely to occur in the flow near hot spots, and nighttime lightning observations will help constrain the regions of upwelling.

Although the models of indirect circulations presented here were created to answer specific questions posed by Galileo data, they may have broader implications. Indirect circulations could play a central role in Jupiter's energetic cycle. The quasi-horizontal nature of atmospheric flows suggests that energy cascades from small to large scales (Charney 1971), contrary to the situation in three-dimensional flows. A sink for kinetic energy must therefore exist at the largest scales; otherwise, energy supplied by thunderstorms, baroclinic instabilities, or other sources at small scales would "pile up" at the largest scales and lead to continuous acceleration of the zonal jets. On Earth, friction against the surface removes much of this large-scale kinetic energy (Peixoto and Oort 1992, Tomatsu 1979), but the lack of a surface on Jupiter suggests that different mechanisms may be at work. Indirect circulations could provide the necessary sink on Jupiter, and it is therefore important to understand their dynamics.

ACKNOWLEDGMENTS

We thank J. Cho, D. Hinson, P. Mahaffy, P. J. Gierasch, N. Renno, G. Schubert, A. Vasavada, and R. Young for useful discussions and D. H. Atkinson and A. Seiff for sharing their preliminary data. W. M. Folkner, R. Woo, H. Niemann, and the mass spectrometer team graciously allowed us to present the data shown in Fig. 1. This work was supported by NASA Grant NAGW-1956 and by the Galileo project.

REFERENCES

Atreya, S. 1996. In *International Conference on the Shoemaker–Levy 9 Jupiter Collision,* p. 2. Observatoire de Paris.

Atreya, S. K., and P. N. Romani 1985. In *Planetary Meteorology* (G. Hunt, ed.), p. 17. Cambridge Univ. Press, Cambridge, UK.

Atreya, S., M. H. Wong, T. Owen, H. Niemann, and P. Mahaffy 1996. Chemistry and clouds of the atmosphere of Jupiter: A Galileo perspective. In *Three Galileos: The Man, the Spacecraft, the Telescope* (conference proceedings) (J. Rahe, C. Barbieri, T. Johnson, A. Sohus, Eds.) Kluwer Academic, Dordrecht.

Atkinson, D. H., J. B. Pollack, and A. Seiff 1996. Galileo Doppler measurements of the deep zonal winds at Jupiter. *Science* **272,** 842–843.

Atkinson, D. H., A. P. Ingersoll, and A. Seiff 1997. Deep zonal winds on Jupiter: Update of Doppler tracking the Galileo probe from the orbiter. *Nature* **388,** 649–650.

Betts, A. K. 1973. Non-precipitating convection and its parameterization. *Quart. J. Roy. Meteor. Soc.* **99,** 178–196.

Carlson, B. E., A. A. Lacis, and W. B. Rossow 1994. Belt-zone variations in the jovian cloud structure. *J. Geophys. Res.* **99,** 14,623–14,658.

Carlson, R., and 39 colleagues 1996. Near-infrared spectroscopy and spectral mapping of Jupiter and the galilean satellites: Results from Galileo's initial orbit. *Science* **274,** 385–388.

Charney, J. G. 1971. Geostrophic turbulence. *J. Atmos. Sci.* **28,** 1087–1095.

Conrath, B. J., D. Gautier, R. A. Hanel, and J. S. Hornstein 1984. The helium abundance of Saturn from Voyager measurements. *Astrophys. J.* **282,** 807–815.

Drossart, P., and 11 colleagues 1997. The solar reflected component in Jupiter's 5 micron spectra from NIMS/Galileo observations. *J. Geophys. Res.*, submitted.

Emanuel, K. A. 1994. *Atmospheric Convection,* Oxford Univ. Press, New York.

Engel, S., D. M. Hunten, A. S. Ackerman, and O. B. Toon 1996. A whiff of cloud on Jupiter. *Bull. Amer. Astron. Soc.* **28,** 1141. [Abstract]

Folkner, W. M., R. Woo, and S. Nandi 1998. Ammonia abundance in Jupiter's atmosphere derived from the attenuation of the Galileo probe's radio signal. *J. Geophys. Res*., submitted.

Folkner, W. M., R. A. Preston, J. S. Border, J. Navarro, W. E. Wilson, and M. Oestreich 1997. Earth-based radio tracking of the Galileo probe for Jupiter wind estimation. *Science* **275,** 644–646.

Garratt, J. R. 1992. *The Atmospheric Boundary Layer.* Cambridge Univ. Press, New York.

Gautier, D., and T. Owen 1989. The composition of outer planet atmospheres. In *Origin and Evolution of Planetary and Satellite Atmospheres* (S. K. Atreya, J. B. Pollack, and M. S. Matthews, Eds.). University of Arizona Press, Tucson.

Gierasch, P. J., B. J. Conrath, and J. A. Magalhaes 1986. Zonal mean properties of Jupiter's upper troposphere from Voyager infrared observations. *Icarus* **67,** 456–483.

Guillot, T. 1995. Condensation of methane, ammonia, and water and the inhibition of convection in giant planets. *Science* **269,** 1697–1699.

Guillot, T. 1996. A parallel between the results of the Galileo probe and the abundance of methane in Uranus and Neptune. *Bull. Amer. Astron. Society* **28,** 1142. [Abstract]

Haltiner, G. J., and R. T. Williams 1980. *Numerical Prediction and Dynamic Meteorology.* Wiley, New York.

Holton, J. R. 1992. *An Introduction to Dynamic Meteorology.* Academic Press, New York.

Holton, J. R., P. H. Haynes, M. E. McIntyre, A. R. Douglass, R. B. Rood, and L. Pfister 1995. Stratosphere–troposphere exchange. *Rev. Geophys.* **33,** 403–439.

Hunten, D. M., M. Tomasko, and L. Wallace 1980. Low-latitude thermal structure of Jupiter in the region 0.1–5 bars. *Icarus* **43,** 143–152.

Ingersoll, A. P., and C. C. Porco 1978. Solar heating and internal heat flow on Jupiter. *Icarus* **35,** 27–43.

Lindal, G. F., and 11 colleagues 1981. The atmosphere of Jupiter: An analysis of the Voyager radio occultation measurements. *J. Geophys. Res.* **86,** 8721–8727.

Mahaffy, P. 1996. Recent calibration studies of the Galileo probe neutral mass spectrometer. *Eos* (Fall suppl.), **77,** F438.

Niemann, H. B., and 12 colleagues 1996. The Galileo probe mass spectrometer: Composition of Jupiter's atmosphere. *Science* **272,** 846–849.

Niemann, H. B., and 11 colleagues 1997. The composition of the jovian atmosphere as determined by the Galileo probe mass spectrometer. *J. Geophys. Res.*, submitted.

Ortiz, J. L., G. S. Orton, A. J. Friedson, S. T. Stewart, B. M. Fisher, and J. R. Spencer 1997. Evolution and persistence of 5-μm hot spots at the Galileo probe entry latitude. *J. Geophys. Res.*, in press.

Orton, G., and 40 colleagues 1996. Earth-based observations of the Galileo Probe entry site. *Science* **272,** 839–840.

Orton, G. S., B. M. Fisher, S. T. Stewart, J. L. Ortiz, M. Marinova, S. Hinkley, V. Krishnan, M. Masanovic, J. Tesic, and A. Tziolas 1997. Characteristics of Galileo probe entry site from Earth-based remote sensing observations. *J. Geophys. Res.*, submitted.

Owen, T. C., and 11 colleagues 1996. *Eos* (Spring suppl.) **77,** S171.

Peixoto, J. P., and A. H. Oort 1992. *Physics of Climate,* American Institute of Physics, New York.

Ragent, B., D. S. Colburn, P. Avrin, and K. A. Rages 1996. Results of the Galileo probe nephelometer experiment. *Science* **272,** 854–856.

Ragnet, B., D. S. Colburn, K. A. Rages, T. C. D. Knight, P. Avrin, G. S. Orton, and G. W. Grams. The clouds of Jupiter: Results of the Galileo Jupiter Mission probe nephelometer experiment. *J. Geophys. Res*., submitted.

Renno, N. O, and A. P. Ingersoll 1995. Natural convection as a heat engine—A theory for CAPE. *J. Atmos. Sci.* **53,** 572–585.

Roos-Serote, M. C., and 12 colleagues 1997. Analysis of Jupiter NEB hot spots in the 4–5 micron range from Galileo/NIMS observations: Measurements of cloud opacity, water, and ammonia. *J. Geophs. Res.*, submitted.

Salby, M. L. 1996. *Fundamentals of Atmospheric Physics,* Academic Press, New York.

Seiff, A., R. C. Blanchard, T. C. D. Knight, G. Schubert, D. B. Kirk, D. Atkinson, J. D. Mihalov, and R. E. Young 1997a. Wind speeds measured in the deep jovian atmosphere by the Galileo probe accelerometers. *Nature* **388,** 650–652.

Seiff, A., D. B. Kirk, T. C. D. Knight, J. D. Mihalov, R. C. Blanchard, R. E. Young, G. Schubert, U. von Zahn, G. Lehmacher, F. S. Milos, and J. Wang 1996. Structure of the atmosphere of Jupiter: Galileo probe measurements. *Science* **272,** 844–845.

Seiff, A., D. B. Kirk, T. C. D. Knight, R. E. Young, J. D. Mihalov, L. A. Young, F. S. Milos, G. Schubert, R. C. Blanchard, and D. Atkinson 1997b. Thermal structure of Jupiter's atmosphere near the edge of a 5-micron hot spot in the north equatorial belt. *J. Geophys. Res*., in press.

Sromovsky, L. A., F. A. Best, A. D. Collard, P. M. Fry, H. E. Revercomb, R. S. Freedman, G. S. Orton, J. L. Hayden, M. G. Tomasko, and M. T. Lemmon 1996. Solar and thermal radiation in Jupiter's atmosphere: Initial results of the Galileo probe net flux radiometer. *Science* **272,** 851–854.

Sromovsky, L. A., A. D. Collard, P. M. Fry, G. S. Orton, M. T. Lemmon, M. G. Tomasko, and R. S. Freedman 1997. Galileo probe measurements of thermal and solar radiation fluxes in the jovian atmosphere. *J. Geophys. Res.*, submitted.

Stewart, S. T., G. S. Orton, B. M. Fisher, and K. H. Baines 1997. The cloud structure of the jovian north equatorial zone: Context of the Galileo probe entry latitude. *J. Geophys. Res.*, submitted.

Tomatsu, K. 1979. Spectral energetics of the troposphere and lower stratosphere. *Adv. Geophysics* **21,** 289–405.

Turner, J. S. 1973. *Buoyancy Effects in Fluids.* Cambridge Univ. Press, Cambridge, UK.

Vasavada, A. R., and 12 colleagues 1997. Galileo imaging of Jupiter's atmosphere: the great red spot, equatorial region and white ovals. *Icarus*, submitted.

von Zahn, U., and D. M. Hunten 1996. The helium mass fraction in Jupiter's atmosphere. *Science* **272,** 849–851.

Weidenschilling, S. J., and J. S. Lewis 1973. Atmospheric and cloud structures of the jovian planets. *Icarus* **20,** 465–476.

West, R. A., A. J. Friedson, and J. F. Appleby 1992. Jovian large-scale stratospheric circulation. *Icarus* **100,** 245–259.

Young, R. E. 1997. The Galileo probe mission to Jupiter: Science overview. *J. Geophys. Res.*, submitted.